Available online at www.sciencedirect.com
ScienceDirect
Geoderma 135 (2006) 1–15
GEODERMA
www.elsevier.com/locate/geoderma

Surface and micropore properties of saline soil profiles

Grzegorz Jozefaciuk [a,*], Tibor Toth [b], Geza Szendrei [c]

[a] Institute of Agrophysics of Polish Academy of Sciences, Doswiadczalna 4, 20-290 Lublin, Poland
[b] Research Institute for Soil Science and Agricultural Chemistry of the Hungarian Academy of Sciences, Herman Otto 15, H-1525 Budapest, Hungary
[c] Natural History Museum of Hungary, Budapest, Hungary

Received 1 March 2005; received in revised form 21 September 2005; accepted 23 October 2005
Available online 4 January 2006

Abstract

Based on water vapor adsorption–desorption isotherms, the specific surface and its energetic and geometric properties were estimated for twelve profiles of saline soils of different salinity. The contents of clay fraction and organic matter governed the CEC and the surface area of the soils. The contribution of clay fraction to the CEC was over four times smaller than that of the organic matter, whereas the contribution of clay to surface area was around three times larger. The average water vapor adsorption energy decreased logarithmically with the increase of the sodium adsorption ratio and linearly with the increase of pH. The amount of soil micropores increased with the increase in surface area. The surface fractal dimension appeared to positively correlate with soil CEC.

Keywords: Adsorption energy; Fractal dimension; Microporosity; Saline soils; Surface area

1. Introduction

Energetic and geometric properties of soil surface become increasingly used for description and modeling of soil physical, chemical and biological processes as well as for quantitative analysis of soil typological and genetic properties. Due to extremely complex mineral, organic and ionic composition of the soil solid, its surface is highly non-uniform. Among many methods developed to study such surfaces an analysis of adsorption–desorption isotherm is probably the easiest and most convenient one (Gregg and Sing, 1967). The adsorption isotherm is a function relating the amount of adsorbed gas (vapor) to its equilibrium pressure during the pressure increase at a constant temperature. The desorption isotherm is the same function measured during the pressure decrease.

From adsorption data one easily estimates an overall amount of the surface i.e. the surface area (specific surface) of the soil adsorbent. The idea of the estimation of the surface area is to find a number of adsorbate molecules that cover the adsorbing surface as a monolayer, and to multiply this number by the area occupied by a single molecule.

Surface heterogeneity can be characterized from energetic point of view by an adsorption energy distribution function. This function, showing amounts (fractions) of surface sites of different adsorption energies, is estimated assuming that different surface sites bind adsorbate molecules with different forces (and energies) thus influencing adsorption pathways. Knowing that at

* Corresponding author. Fax: +48 81 7445067.
E-mail addresses: jozefaci@demeter.ipan.lublin.pl (G. Jozefaciuk), tibor@rissac.hu (T. Toth).

0016-7061/$ - see front matter © 2005 Elsevier B.V. All rights reserved.
doi:10.1016/j.geoderma.2005.10.007

Table 1
Characteristics of the studied sites

Locality	Sarrod	Egerlovo	Szabadkigyos	Zam puszta
Abbreviation	SA	EG	SZ	ZA
Northern	47°39.253′	47°43.600′	46°36.232′	47°31.669′
Eastern	16°48.764′	20°35.706′	21°5.815′	21°2.381′
Soil type	Stagnic Solonchak	Vertic Solonetz	Mollic Solonetz	Haplic Solonetz
Use	Grassland	Grassland	Grassland	Grassland
Elevation (m)	118	95	91	94
Native plants	*Salicornea europea*, *Suaeda salsa*, *Plantago maritima*	*Suaeda salsa*, *Limonium gmelini*, *Artemisia santonicum*	*Camphorosma annua*, *Puccinellia limosa*, *Artemisia santonicum*	*Salicornea europea*, *Suaeda salsa*, *Plantago maritima*
gw D (cm)	190	180	204	250
gw EC	6.0	1.5	5.0	7.5
gw pH	7.7	7.8	8.0	8.1
gw SAR	19	4	68	65
gw Ca^{2+}*	2.5	2.5	0.32	0.38
gw Mg^{2+}*	9	1.5	0.5	2.0
gw Na^{+}*	66	9	61	100
gw K^{+}*	0.25	0.24	0.07	1
gw SO_4^{2-}*	34	4.5	4.5	0.5
gw Cl^{-}*	16	1	27	73
gw CO_3^{2-}*	2	1	3.5	1
gw HCO_3^{-}*	7	20	26	19.4
Locality	Ujfeherto	Peterito	Alap	Akaszto
Abbreviation	UJ	PE	AL	AK
Northern	47°47.795′	46°34.635′	46°48.927′	46°40.578′
Eastern	21°41.250′	19°53.984′	18°39.503′	19°9.121′
Soil type	Stagnic Solonchak	Gleyic Solonchak	Calcic Solonchak	Salic Solonetz
Use	Grassland	Grassland	Grassland	Grassland
Elevation (m)	114	93	92	94
Native plants	*Kochia scoparia*, *Puccinellia limosa*	*Puccinellia limosa*, *Lepidium crassifolium*, *Aster tripolium*	Camphorosma annua, *Limonium gmelini*	Lepidium crassifolium, *Puccinellia limosa*
gw D (cm)	150	80	200	95
gw EC	4.7	11.0	11.0	7.5
gw pH	8.15	8.3	8.2	9.6
gw SAR	45	90	80	145
gw Ca^{2+}*	0.5	0.05	0.7	0.03
gw Mg^{2+}*	1.25	3.5	3	0.5
gw Na^{+}*	60	169	154	105
gw K^{+}*	0.2	2.3	0.3	0.5
gw SO_4^{2-}*	1.2	0.5	60	3.6
gw Cl^{-}*	5.2	31	37	16
gw CO_3^{2-}*	3.8	18	2.7	23
gw HCO_3^{-}*	60	56	17.3	79
Locality	Karcag	Karcag	Karcag	Karcag
Abbreviation	KA	KB	KC	KD
Northern	47°18.628′	47°18.650′	47°18.606′	47°18.655′
Eastern	20°48.737′	20°49.969′	20°48.632′	20°48.633′
Soil type	Haplic Chernozem	Haplic Chernozem	Haplic Vertisol	Haplic Chernozem
Use	Cropland	Cropland	Cropland	Cropland
Elevation (m)	88	87	86	87
Native plants	na	na	na	na
gw D (cm)	200	200	220	220
gw EC	7.4	5.7	2.8	4.1
gw pH	8.5	8.4	7.7	8.2
gw SAR	49	43	11	24
gw Ca^{2+}*	0.52	0.52	1.45	0.3

Table 1 (*continued*)

Locality	Karcag	Karcag	Karcag	Karcag
gw Mg^{2+}*	2.1	1.87	1.95	1.14
gw Na^{+}*	79.4	67.2	20.9	28.8
gw K^{+}*	0.04	0.03	0.04	0.03
gw SO_4^{2-}*	1.8	2.6	1.1	0.9
gw Cl^{-}*	35.7	14.0	4.41	3.07
gw CO_3^{2-}*	2.3	1.3	0	0.6
gw HCO_3^{-}*	19.4	27.3	8.4	17.7

Abbreviations: gw — groundwater, D — depth, EC — electric conductivity (mS cm^{-1}), SAR — sodium adsorption ratio, * data in mM dm^{-3}, na — not applicable.

the equilibrium the free energy is constant throughout the system, the energy of water vapor at a given relative vapor pressure is associated with adsorption energy on a given site, while the number of given adsorption sites is estimated from the amount adsorbed. From the distribution function one can easily derive an average adsorption energy that characterizes global energetic character of the surface.

Surface area and energetic properties of soil surface are highly sensitive indicators of various processes occurring in soils: organic matter accumulation, leaching and oxidation, soil acidification, alkalization, silica accumulation, wetting–drying cycles and many others (Sokolowska, 1989; Chiou et al., 1990; Wilczynski et al., 1993; Pachepsky et al., 1995a; Pennell et al., 1995; Sequi and Aringhieri, 1977; Balard et al., 1997; Tombacz et al., 1998; Hoffmann et al., 1999; Jozefaciuk and Bowanko, 2002; Coradin and Livage, 2003; Sokolowska et al., 1993a,b, 1997, 1999, 2000; Jozefaciuk et al., 1995, 1996, 2000, 2001, 2003).

Large surface areas of soil adsorbents result from their microporous character. Soil micropore characteristics can be determined from desorption isotherms, assuming that the desorption process is equivalent to an evaporation of the adsorbate condensed in the micropores. The relative vapor pressure during desorption is related to the micropore radius and the amount of the evaporated adsorbate to the pore volume. The first derivative of the pore volume vs. radius function gives pore size distribution, from which the average micropore radius can be calculated.

Micropore characteristics are frequently applied in studies of changes in soil solid under different natural and anthropogenic effects (Hernandez, 2000; Jozefaciuk and Sokolowska, 2003; Hajnos et al., 1999, 2003; Jozefaciuk et al., 2001, 2002, 2003).

From geometric point of view surface heterogeneity may be characterized by a surface fractal dimension. The fractal dimension is a measure of the surface roughness. If a surface is fractal, higher fractal dimension characterizes a rougher one. The basic property of fractal objects is that they are geometrically similar to their parts. Surface fractal dimension can be estimated from dependencies of adsorption vs. adsorption potential, plotted in logarithmic coordinates.

Fractal geometry becomes increasingly used for describing soil structural features and their effect on soil physical, chemical and biological processes (Allen and Hoekstra, 1991; Perfect and Kay, 1995; Pachepsky et al., 1995b; Anderson et al., 1998; Lipiec et al., 1998; Sokolowska and Sokolowski, 1999; Senesi, 2000).

Although it is widely known that salt-affected soils show close relationship between physical and chemical properties, according to the authors knowledge surface properties of saline soils are not well known and described in the literature.

In our previous work (Toth and Jozefaciuk, 2002) we observed that specific features of saline soils affect surface properties of the soil material and their profile distribution. In the above study we used three soil profiles located in the same field and having rather similar properties. The objective of the present paper is to describe surface and micropore characteristics of higher number of sodic and saline profiles of large differences in salinity and relate these properties to factors of soil formation.

2. Materials and methods

Samples taken from genetic horizons of twelve salt-affected Hungarian soil profiles were studied. To cover the largest range of soil salinity we took the samples starting from relatively slightly saline/sodic/alkaline croplands up to the soils having salt efflorescences on the surface. The profiles described in situ using standard field techniques were next analyzed using routine laboratory procedures.

Water vapor adsorption isotherms were measured for the studied samples using vacuum chamber method at a temperature $T = 294 \pm 0.1$ K. To reach different relative water vapor pressures, p/p_0, sulfuric acid of stepwise decreasing concentrations (increase of p/p_0) was used.

Table 2
Selected properties of the studied profiles

Site sampling date	Horizon	Depth (cm)	Wet color	Texture	Structure	Sample name
Sarrod 2000 AUG 29	1	0–10	10YR5/2	SL	s-SUB	SA5
	2	10–18	10YR3/2	C	s-SUB	SA14
	3	18–52	2.5Y7/3	CL	s-SUB	SA35
	4	52–54	10YR4/3	LS	nps	SA53
	5	54-75	2.5Y7/2	CL	nps	SA65
Egerlovo 2000 AUG 9	A/e	0–8	2.5Y3/1	L	PLA	EG4
	B1	8–21	2.5Y2/1	CL	PRI	EG14
	B2	21–46	2.5Y3/1	CL	l-SAB	EG34
	B3	46–78	2.5Y2/1	C	ABL	EG62
	BC	78–118	2.5Y3/1	C	ABL	EG98
	C	118–130	2.5Y4/1	LC	SAB	EG124
Szabadkigyos 2000 SEP 8	A	0–2	10YR4/2.5	L	PLA	SZ1
	B1	2–17	10YR2/1	CL	COL	SZ9
	B2	17–36	10YR2/2	CL	SAB	SZ26
	BC	36–67	2.5Y4/3	CL	PRI	SZ53
	C	67–90	2.5Y4.5/5	CL	PRI	SZ78
Zam puszta 2001 AUG 23	A/e	0–7	2.5Y3/2	L	PRI	ZA3
	B1	7–22	2.5Y3/2	C	s-SAB	ZA14
	B2	22–38	2.5Y3/2	C	ABL	ZA30
	BC	38–68	2.5Y4/2	C	ABL	ZA53
	C1	68–75	2.5Y5/3	C	SAB	ZA71
	C2	100–120	2.5Y5/3	C	SAB	ZA110
Ujfeherto 1999 AUG 16	1	0–4	5Y5/3	SL	PLA	UJ2
	2	4–14	5Y5/3	CL	ABL	UJ9
	3	14–40	2.5Y5/4	L	SAB	UJ27
	4	40–85	2.5Y5/6	L	SAB	UJ62
Peterito 2000 JUL 28	1	0–3	2.5Y4/2	SL	PLA	PE2
	2	3–13	2.5Y5/2	LS	s-SAB	PE8
	3	13–39	2.5Y4/2	LS	s-SAB	PE26
	4	39–58	2.5Y5/2	LS	s-SAB	PE48
	5	58–77	2.5Y6/1	LS	s-SAB	PE68
Alap 2000 AUG 24	1	0–2 (efflor)	7.5YR2/2	SC	nps	AL1
	2	2–28	7.5Y2/2	SC	COL	AL15
	3	28–57	7.5Y3/2	SC	SAB	AL43
	4	57–71	2.5Y7/4	SG	SAB	AL64
	5	71–82	2.5Y7/6	SL	SAB	AL76
Akaszto 1998 JUL 30	A	0–3	5Y5/2	SL	s-SAB	AK2
	B	3–19	5Y6/2	CL	COL	AK11
	BC	19–38	5Y6/3	L	SAB	AK28
	C1	38–58	5Y6/3	L	SAB	AK48
	C2	58–90	5Y6/3	L	SAB	AK74
	C3	90–92	5Y5/3	LS	SAB	AK92
Karcag KA 1998 OCT 22	Ap	0–18	10YR3/1	CL	ABL	KA9
	A	18–32	10YR3/1	CL	ABL	KA25
	B	32–51	2.5Y3/1	CL	s-SAB	KA42
	BC	51–92	10YR3/2	CL	s-SAB	KA72
	C	92–100	10YR4/3	CL	s-SAB	KA96
Karcag KB 1998 OCT 22	Ap	0–21	10YR2/2	CL	s-SAB	KB11
	A	21–46	10YR3/1	CL	s-SAB	KB33
	B	46–68	10YR3/2	CL	SAB	KB57
	BC	68–111	2.5YR4/2	CL	ABL	KB89
	C	111–118	2.5YR4/3	CL	ABL	KB114
Karcag KC 1998 OCT 22	Ap	0–20	10YR2/1	CL	ABL	KC10
	A	20–36	10YR2/1	CL	PRI	KC28
	B	36–75	10YR2/1	CL	ABL	KC56
	BC	75–95	10YR2/1	CL	PRI	KC85
	C	95–105	10YR3/2	CL	ABL	KC100

Table 2 (*continued*)

Site sampling date	Horizon	Depth (cm)	Wet color	Texture	Structure	Sample name
Karcag KD 1998 OCT 22	Ap	0–28	10YR2/2	CL	ABL	KD14
	A	28–45	10YR2/2	CL	ABL	KD26
	B	45–68	10YR2/2	CL	ABL	KD56
	BC	68–105	10YR3/3	CL	ABL	KD87
	C	111–115	2.5YR4/3	L	ABL	KD113

Abbreviations: SL — sandy loam, L — loam, CL — clay loam, C — clay; PLA — platy, SAB — subangular blocky, ABL — angular blocky, COL — columnar, PRI — prismatic, l — large, s — small, nps — no pedological structure developed.

The amount of adsorbed water, a [kg kg^{-1}], at a given p/p_0 was measured after 48 h of equilibration by weighing. Similarly, water vapor desorption isotherms were measured, but sulfuric acid of stepwise increasing concentrations (decrease of p/p_0) was used. The dry mass of the samples was estimated after completing the measurements of both isotherms by 24 h oven drying at 378 K. The measurements were performed in three replicates. The deviation between experimental points depended on the relative water vapor pressure. During desorption cycle, at p/p_0 values higher than 0.8 this was up to 5% and at p/p_0 values lower than 0.3 less than 1%. The adsorption data were better reproducible.

From the experimental adsorption and desorption data specific surface areas, adsorption energy distribution functions, average adsorption energies, micropore size distribution functions, average micropore radii, micropore volumes and surface fractal dimensions were calculated as described in the Appendix.

3. Results and discussion

Basic properties of the studied soils are collected in Tables 1–3. Table 3 contains also the surface and micropore characteristics estimated from the isotherms.

The studied profiles were collected in different regions of the Hungarian Plain, a floodplain with varying thickness of alluvial sediments. Occurrence of salt-affected soils is closely related to groundwater depth and salinity, being the most important factors of salinization, and also to surface waters — the frequency and time of waterlogging. During the last two hundred years great changes in the hydrological situation in the Plain took place and the distribution of salt-affected soils reflects these changes closely (Toth et al., 2001). At most of the sampling sites the groundwater level has been sufficiently close to the surface and enough saline to cause salt accumulation.

Very slightly salt-affected Karcag (K) profiles represent the best stands for crops: Chernozems (KA (irrigated), KB and KD) and a Vertisol (KC, a site at lower elevation, irrigated). The native vegetation on higher areas are thick grasses and the soil is fertile. In the lowest patches fine particles have been settled and the soil is cracking, but also undergoes frequent waterlogging. As it is typical for such soils, sodicity is observed only in deeper layers of the subsoil (where the capillary water-rise affects the chemical features) and the topsoil is salt-free.

Among the other soils (taken from native sites), some occurred at relatively higher elevation in the toposequence (Egerlovo EG, Szabadkigyos SZ and Alap AL) where the salt efflorescences can be found in small patches only. Solonetz is the typical soil type in this situation, but Solonchak limited to small patches is found also. The latter soil type is most frequent in waterlogged areas and beside saline lakes. The above soils have *Artemisia santonicum* as the dominant plant species. Intermediate elevation site at Akaszto (AK) was earlier a temporary lake, already being dried out and covered by sparse vegetation stands of *Camphorosma annua*. From lower elevations we sampled Ujfeherto (UJ) and Zam (ZA) profiles, temporary waterlogged, where *Kochia scoparia* and *Salicornia europea* are characteristic plant species, respectively. The lowest elevation sites (Sarrod SA and Peterito PE) are close to typically saline lakes, where *Suaeda salsa* and *Aster tripolium* plus *Puccinellia limosa* (more hydrophytic vegetation) dominate, respectively, although these soils are not usually covered by lake water.

The drier, upland sites of highly saline soils are grazed by sheep and the lowland ones, especially those beside lakes, are grazed by wild geese.

Chernozem and Vertisol profiles at Karcag are more brown (10YR) than salt-affected soils. Profiles close to lakes are paler in colors. The variable layering of the subsoil of SA profile, caused by depositions, is evidenced in color and texture as well.

The texture of the studied soils ranges from loamy sand to clay. The eluvial A/E horizons of Solonetz soils have coarser texture and a higher clay content than the illuvial horizons. In Solonetz soils prismatic and columnar structure reflects high sodicity. The amount of clay in soils of higher salinity is usually the highest in

Table 3
Chemical and surface characteristics of the studied soils

Sample	pH	OM	Carb.	Clay	CEC	SP	EC	Na	SAR	*S*	*D*	*E*/*RT*	*r*	Vp
SA5	8.98	0.89	22.1	15.0	6.1	33	27.0	345	45.1	51.0	2.48	−2.92	13.9	37.1
SA14	8.93	0.93	33.7	38.1	12.9	62	16.2	167	33.5	90.5	2.64	−2.88	16.8	48.4
SA35	8.94	0.56	57.9	45.0	10.6	55	15.3	162	30.8	61.4	2.54	−2.82	17.4	43.1
SA53	9.21	0.48	26.6	17.8	7.9	33	11.2	110	26.5	48.4	2.65	−2.86	15.2	24.3
SA65	9.13	0.42	53.7	36.6	8.6	57	11.6	111	26.2	53.6	2.58	−2.92	15.2	31.8
EG4	8.08	4.31	1.3	29.4	25.4	66	25.2	440	69.7	144	2.74	−2.98	14.2	82.0
EG14	8.66	2.33	9.0	50.6	32.3	93	21.0	342	64.2	208	2.74	−2.61	16.4	102
EG34	9.11	1.55	14.8	50.0	32.0	128	14.0	192	73.6	199	2.73	−2.59	15.2	102
EG62	9.14	1.30	13.3	46.9	31.4	143	8.0	97	71.0	173	2.75	−2.50	16.5	87.1
EG98	9.24	0.99	12.6	42.2	28.3	140	2.7	28	40.8	165	2.76	−2.54	14.7	74.9
EG124	9.39	0.71	28.2	38.1	22.3	98	2.5	11.2	21.8	104	2.80	−2.92	17.1	49.6
SZ1	9.26	2.20	4.24	30.0	23.6	53	21.0	380	223	108	2.75	−2.64	14.5	53.1
SZ9	9.56	2.37	12.7	44.5	26.3	67	25.4	456	357	154	2.64	−2.61	16.6	87.6
SZ26	9.80	1.74	18.2	41.1	23.7	69	19.5	345	361	127	2.68	−2.59	16.0	68.2
SZ53	9.92	1.18	20.4	38.5	20.4	73	11.8	187	258	97.9	2.66	−2.69	16.5	57.2
SZ78	9.97	0.59	22.9	37.1	16.0	86	6.9	100	171	87.7	2.65	−2.47	15.9	51.3
ZA3	9.21	2.05	0.3	28.5	18.2	52	36.2	489	409	83.4	2.48	−2.26	15.1	89.1
ZA14	9.68	1.56	0.3	34.7	21.8	66	22.8	289	282	119	2.58	−2.32	15.9	89.8
ZA30	9.75	1.41	0.8	44.9	25.6	93	16.3	200	249	197	2.63	−2.43	14.4	97.5
ZA53	9.73	1.00	5.6	48.2	25.7	116	10.5	117	137	147	2.58	−2.26	13.6	106
ZA71	9.72	0.84	21.4	44.3	19.5	98	8.3	87	110	96.9	2.52	−2.30	16.6	94.0
ZA110	9.48	0.49	20.6	33.6	16.6	88	7.2	75	77.4	178	2.45	−2.01	16.2	76.3
UJ2	10.2	0.79	6.72	10.3	6.3	37	20.0	405	684	37.2	2.61	−2.70	17.6	28.2
UJ9	10.4	0.40	11.13	21.8	9.0	44	8.0	138	223	44.9	2.62	−2.68	18.0	30.8
UJ27	10.3	0.38	36.8	28.8	11.0	57	4.7	82	160	48.6	2.63	−2.72	19.2	36.2
UJ62	10.3	0.21	26.25	22.8	11.0	50	3.5	62	111	46.2	2.66	−2.82	17.4	28.1
PE2	9.95	1.29	15.2	7.1	5.2	37	71	1080	620	26.2		−1.83	18.5	72.3
PE8	10.2	0.69	20.2	10.7	3.7	33	7.9	100	197	20.9	2.56	−2.98	16.1	16.9
PE26	10.4	0.30	13.5	9.8	3.9	33	6.3	80	169	24.3	2.49	−2.69	20.2	21.4
PE48	10.4	0.22	20.2	15.8	3.8	47	6.2	75	180	17.5	2.43	−2.46	17.6	19.5
PE68	10.3	0.22	31.6	20.4	3.9	44	6.2	74	136	16.8	2.44	−2.77	18.4	20.2
AL1	9.87	1.18	2.5	14.2	8.3	33	78	1750	2060	30.0	2.32	−1.59	17.1	58.0
AL15	9.84	1.17	4.2	22.7	15.2	48	25.0	386	387	77.6	2.44	−2.45	12.0	56.0
AL43	10.0	0.68	16.9	21.7	9.6	46	16.2	220	339	40.4	2.43	−2.47	12.7	28.6
AL64	10.2	0.06	13.9	4.2	3.8	33	10.0	124	560	25.7	2.43	−2.22	15.3	17.2
AL76	9.87	0.16	23.2	17.2	10.5	73	9.5	114	260	63.0	2.48	−2.34	12.8	28.5
AK2	9.88	1.19	29.3	9.2	5.4	35	70	1000	2100	27.8	2.47	−3.12	18.1	49.7
AK11	10.2	0.63	33.9	20.1	7.3	39	29.0	398	3370	48.4	2.58	−3.10	16.4	40.5
AK28	10.1	0.20	38.2	17.8	7.3	43	27.5	374	7780	44.5	2.48	−3.32	17.9	51.1
AK48	10.1	0.23	33.9	13.0	7.5	40	24.3	329	10,000	41.7	2.59	−3.06	17.3	36.3
AK74	10.5	0.23	26.3	3.0	5.8	35	12.7	120	10,000	29.0	2.70	−2.51	12.6	12.7
AK92	10.5	0.13	18.7	3.6	4.9	30	12.8	134	484	21.6	2.69	−2.72	11.0	12.3
KA9	7.33	5.32	0.0	41.3	26.7	47	1.1	3.8	2.05	71.9	2.68	−3.04	16.2	36.1
KA25	6.91	4.08	0.0	40.8	33.3	46	0.7	2.3	1.69	104	2.64	−3.36	12.3	50.4
KA42	7.67	3.15	1.4	41.4	34.5					126	2.76	−3.73	15.0	58.1
KA72	8.51	2.59	7.2	41.7	33.2	52	0.5	3.6	5.19	111	2.67	−3.69	14.7	55.5
KA96	9.52	0.94	8.8	39.3	15.7	51	1.2	12	19.0	97.9	2.70	−3.31	14.6	54.2
KB11	7.40	6.48	0.0	40.2	24.3	48	0.8	2.7	1.62	110	2.73	−3.79	11.1	50.0
KB33	7.84	2.99	1.2	39.5	24.4	52	0.6	2.5	1.94	120	2.75	−3.92	12.3	50.5
KB57	8.38	2.54	5.8	40.3	27.3	53	0.5	2.9	3.08	117	2.79	−3.68	15.0	54.3
KB89	9.25	1.83	9.5	40.3	17.0	47	1.0	9.3	13.4	99.5	2.64	−3.48	12.7	49.1
KB114	9.72	0.07	9.9	35.9	14.0	56	2.1	22	30.7	86.6	2.58	−2.95	14.1	53.5
KC10	7.47	5.61	0.0	39.0	24.1	48	0.6	3.5	3.46	103	2.66	−3.70	12.9	55.5
KC28	7.67	3.87	0.0	40.1	21.6	45	0.7	5.6	6.55	108	2.66	−3.72	14.1	53.5
KC56	8.76	2.91	0.0	49.0	31.8	46	1.2	11	15.9	130	2.67	−3.56	12.5	61.3
KC85	8.95	1.99	0.0	47.8	29.8	49	2.6	27	31.1	123	2.67	−3.21	12.6	67.8
KC100	8.97	1.22	0.0	46.6	19.6	55	2.6	27	33.2	112	2.59	−3.03	12.0	62.3
KD14	7.53	5.42	0.0	40.1	27.7	48	1.1	9.1	10.0	113	2.74	−3.59	17.1	56.0

Table 3 (*continued*)

Sample	pH	OM	Carb.	Clay	CEC	SP	EC	Na	SAR	*S*	*D*	*E*/*RT*	*r*	Vp
KD26	7.39	3.37	0.0	40.3	31.5	53	0.6	3.0	2.92	124	2.68	−3.56	11.3	65.5
KD56	8.05	2.71	4.9	38.5	22.3	55	0.5	2.2	2.05	113	2.72	−3.45	14.5	53.1
KD87	8.28	2.02	8.8	39.8	18.8	52	0.5	2.9	3.34	101	2.71	−3.64	11.9	47.0
KD113	9.03	1.54	11.4	37.8	20.3	46	0.7	6.0	8.81	91.6	2.69	−3.52	9.2	43.1

Abbreviations: pH H_2O, OM — organic matter %, Car. — carbonates %, Clay — clay %, SP — saturation percentage, EC — electric conductivity of the soil saturation extract (mS cm^{-1}), Na — sodium concentration in the soil saturation extract (mM dm^{-3}), SAR — sodium adsorption ratio, *S* — specific surface area (m^2 g^{-1}), *D* — fractal dimension, *E*/*RT* — adsorption energy (expressed in units of the thermal energy, *RT*), *r* — average micropore radius (nm), Vp — micropore volume (mm^3 g^{-1}).

illuvial B horizons while in low saline or no saline soils this is rather uniform throughout the whole profile.

The presence of calcium carbonate is common all over the Hungarian Plain because of the frequent occurrence of loessial and carbonatic deposits of River Danube. All studied profiles contain carbonates except the Vertisol KC. As it is typical for Chernozems, calcium carbonate occurs in deeper layers in KA, KB and KD. Leached (low carbonate) topsoil layers are characteristic for Solonetz soils, whereas Solonchaks contain rather high amounts of carbonates right at the surface.

Electrical conductivity of the saturated soil extracts ranges between 2 and 78 dS/m for salt-affected soils and this is significantly lower for slightly salt-affected soils. Solonchak soils show continuously decreasing EC values down the horizon. Solonetz soils show small electric conductivities at the surface and a maximum in B2 horizons. In non-saline soil types (Chernozem and Vertisol) the largest EC values are found in the deepest horizon, which resulted mostly from groundwater salinity. The sodium adsorption ratio decreases in general with the profile depth except of no saline Karcag profiles and the AK profile of the highest salinity.

All but one horizon samples are alkaline and reach pH values higher than 9 in most cases. More leached horizons of slightly saline and Solonetz profiles can have neutral pH at the surface. Soil pH increases down the profiles, similarly as the carbonates.

As a minimal value, soil organic matter of 0.8% was determined. Solonchak soils typically do not have SOM larger than 1.5%. SOM content around 3% can be found in the uppermost horizon of Solonetz soils. Chernozem and Vertisol profiles show SOM above 5%. The amount of soil organic matter accumulated in the studied profiles is closely related to their pH as it is illustrated in Fig. 1. Presence of such dependence was very surprising for us, because the amount of soil organic matter in soils depends on many environmental factors, conditions of soil genesis and physical soil properties, and not on a single parameter. However all studied soils are located within that same physiographic area and, as far as the pH is a main parameter responsible for organic matter leaching, one may suspect that at higher pH the organic matter accumulation has been prevented. Also, the extremely harmful conditions for plants and microbes in high pH soils may play a role: less plants leave less residues and soil organic matter content is smaller. Lower pH values at native sites are due to better vegetation, as well: plants use basic cations that results in pH decrease.

Cation exchange capacity in the studied soils depends both on the amount of clay and organic matter. Good linear fit is obtained for the first relation (CEC = 0.60clay − 1.1; R^2 = 0.72) and much worse for the second one (CEC = 4.2OM + 10.8; R^2 = 0.44). The CEC against OM dependence increases faster at low OM contents and then slower with OM increase which indicates that the higher the amount of organic matter, the lower the CEC of its unit mass. This certifies also that organic matter in saline soils (in which the amount

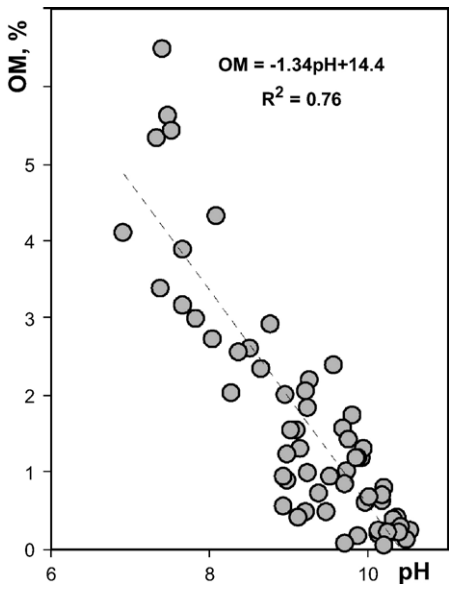

Fig. 1. Dependence of the amount of organic matter (OM) on pH for the studied soils.

of organic matter is smaller) has higher exchange capacity than in no saline ones, as this was postulated by Toth and Jozefaciuk (2002). Very good linear fit between CEC and both clay and organic matter content was obtained from multiple regression analysis ($CEC = 0.49 * (clay + 4.4 \times OM) - 1.0$; $R^2 = 0.81$). The dependencies mentioned above are shown in Fig. 2. It may be concluded that the input of organic material to the CEC in the studied soils is over four times larger than that of the clay. However throughout the literature one finds CEC values of soil organic components from a few hundreds to over 1000 cM kg^{-1} that is over 10 times larger than that of mineral clay components (usually from few tens to rarely over 100 cM kg^{-1}).

Typical water vapor adsorption curves for the studied soil profiles are presented in Fig. 3. Desorption branch is depicted only for this soil horizon, which represents the highest adsorption to have more clear drawings. In all cases, adsorption–desorption hysteresis loops are not large and start at about $p/p_0 = 0.2$–0.4. In general, the highest adsorption occurs in B horizons. All studied isotherms are of the IInd type according to the BET classification that is typical for polymolecular adsorption. However, in dried saline soils salt precipitates may occur, thus at least some of water vapor molecules may undergo rather dissolution than adsorption. There may be insurmountable difficulties of distinguishing between adsorbing and dissolving surfaces.

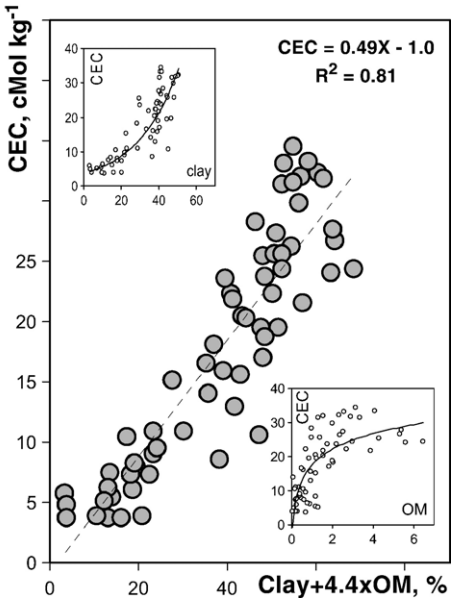

Fig. 2. Dependence of soil cation exchange capacity on cumulative content of clay and organic matter (OM) obtained from multiple regression analysis. Individual dependencies are shown in small pictures within.

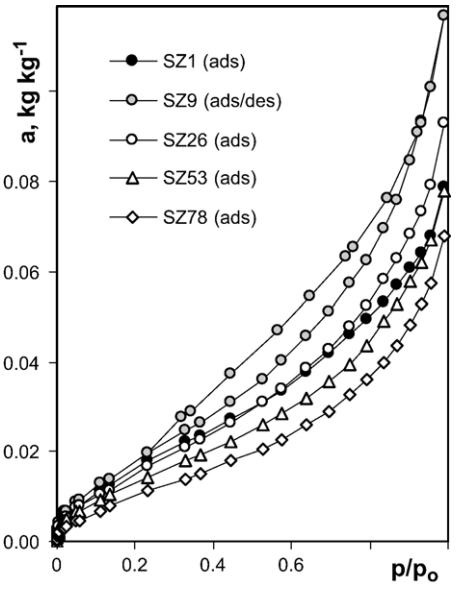

Fig. 3. Typical adsorption isotherms for the studied soils. For S9 sample (maximum adsorption) the desorption isotherm is depicted also. Samples' abbreviations as in Table 2.

We thought to wash out all salts but in this case the surface ionic composition of saline soils would approach that of non-saline ones due to better electrostatic adsorption of polyvalent cations at increasing surface potential during ionic strength decrease. Also using homoionic samples, as this is frequently done, is useless. Therefore to better approach the natural sorption processes we decided to study the soils as these were sampled. Nevertheless, a great care should be taken in the interpretation of surface parameters.

Typical adsorption energy distribution functions are illustrated in Fig. 4. For all soils low energy sites dominate. In most studied horizons a peak at adsorption energy = − 1.5 occurs. All horizons of ZA and AL soils have the highest amount of the lowest adsorption energy sites thus their energy distribution functions resemble that of SA5 sample (illustrated). The energy distributions in other saline soils have similar shapes to the rest of SA samples. The KA, KB, KC and KD soils have higher amounts of higher energy centers and lower amounts of low energy centers than the other soils, that is illustrated for the surface horizon of the KA soil.

The surfaces of the studied soils seem to be fractal as what is seen from the linearity of ln–ln plots of adsorption vs. adsorption potential (fractal plots). Typical example is presented in Fig. 5 for PE soil profile. The slopes of the regression lines (see $1/m$ parameter in Eq. (13), Appendix) indicate that for all studied soils capillary condensation processes are responsible for water vapor adsorption at high relative water vapor pressures.

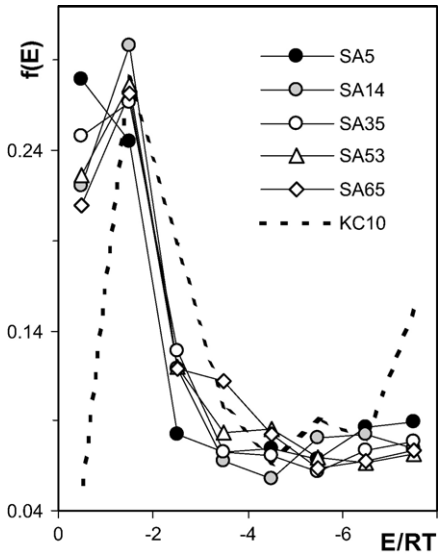

Fig. 4. Typical adsorption energy distribution functions for the studied soils showing fraction of sites (f) of defined adsorption energies (E/RT). Samples' abbreviations as in Table 2.

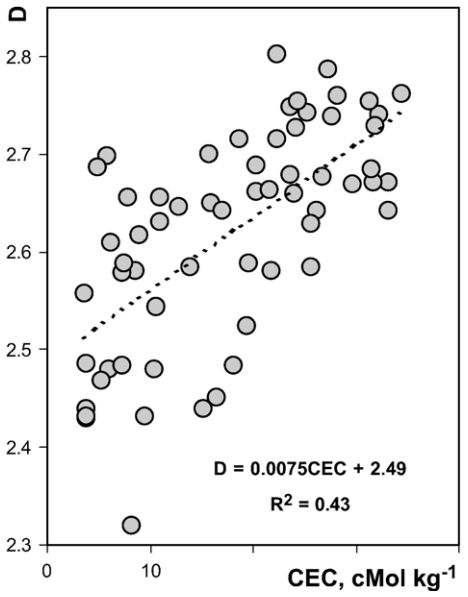

Fig. 6. Dependence of the surface fractal dimension (D) on cation exchange capacity (CEC) for the studied soils.

Micropore fractal dimensions D are rather high (over 2.5 in most cases) indicating that the surfaces (or fine micropores) of the solid material are rough and complicated. The fractal dimension is smallest in the AL soil of the highest salinity. The surface fractal dimension appears to positively correlate with soil CEC, as this is illustrated in Fig. 6. Although the correlation is not satisfactory, this dependence seems interesting because the tendency is rather evident and, according to the authors' knowledge, it has not been observed in other, not salt-affected soils. Due to origin from the same region, the initial materials from which the studied soils were formed could have similar composition, low complicated surfaces and low CEC. Soil formation processes as humus accumulation, mineral weathering and resynthesis might produce solids of more complicated surfaces and higher CEC, as well. Thus the ion exchange positions may be located on most rough parts of the surface, which can explain the above dependence.

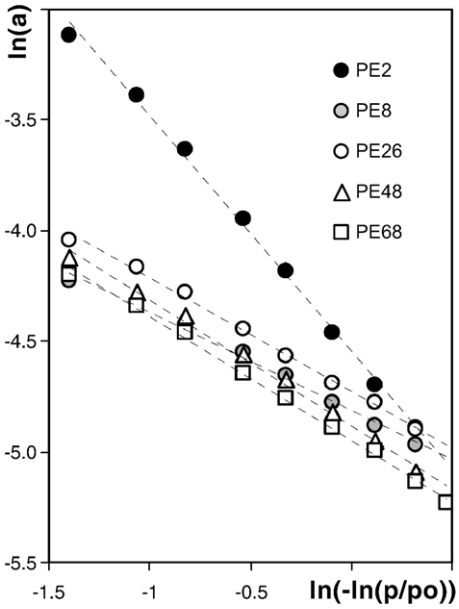

Fig. 5. Exemplary fractal plots for the studied soils. Samples' abbreviations as in Table 2.

Typical micropore size distributions evaluated from desorption isotherms are presented in Fig. 7. Usually the micropores of around 10 μm dominate and around this value a large peak is formed. The second small peak occurs at smaller micropore radii, around 1.8 μm. The latter peak is nearly absent in PE and UJ soils. The micropore radius calculated from the distribution functions exhibited no clear relations with other physical and chemical characteristics of the studied soils.

The surface area of the studied soils increases with an increase of the amount of clay ($S=3.0\text{clay}-3.3$, $R^2=0.69$), however this does not correlate with the organic matter itself ($S=13.5\text{OM}+68$, $R^2=0.17$). Similarly, as for the CEC, good linear fit between S and both clay and organic matter content was obtained from regression analysis ($S=0.97*(\text{OM}+3.0\text{clay})-3.3$, $R^2=0.69$). However, contrary to the CEC, the contribution of clay fraction to surface area is larger than that of organic matter. The surface area is very well corre-

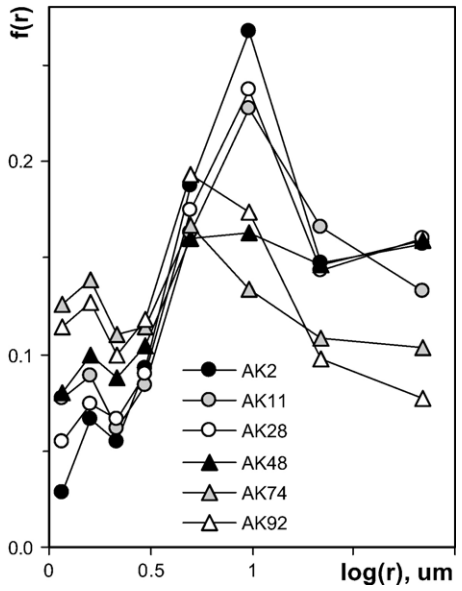

Fig. 7. Typical pore size distribution functions for the studied soils, showing fractions of pores (f) of different radii (r). Due to large range of pore radii, for r-axis logarithmic scale is used. Samples' abbreviations as in Table 2.

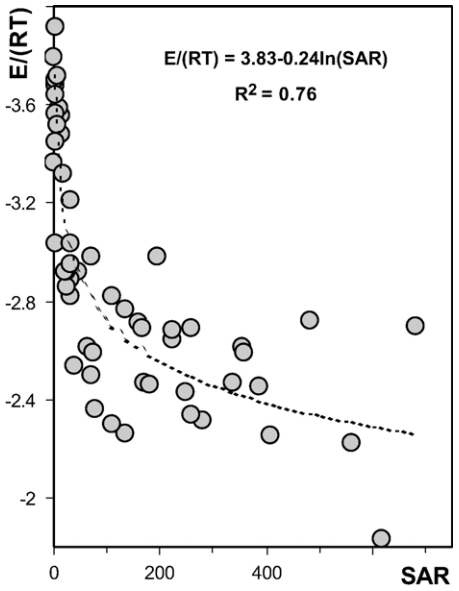

Fig. 9. Dependence of the average adsorption energy (E/RT) on sodium adsorption ratio (SAR) for the studied soils.

lated with soil CEC, as this is illustrated in Fig. 8. Surface cations are dominant water vapor adsorption centers (Newman, 1983). Good correlations of S and CEC have been frequently reported in the literature for no saline (Sokolowska, 1989; Petersen et al., 1996) as well as for saline soils (Toth and Jozefaciuk, 2002). The amount of soil micropores (micropore volume) is well correlated with surface area ($V=0.39S+17.5$, $R^2=0.68$), and this increases with the amount of clay and the CEC of the soils. However, linear fits for both latter dependencies have no high correlation coefficients (R^2 values are around 0.45 in both cases). High surface area (S) and large volume of micropores (V) are well correlated with high water retention in soils (Walczak et al., 2002). In salt-affected soils the exchangeable sodium and pH increase the water retention (Varallyay,

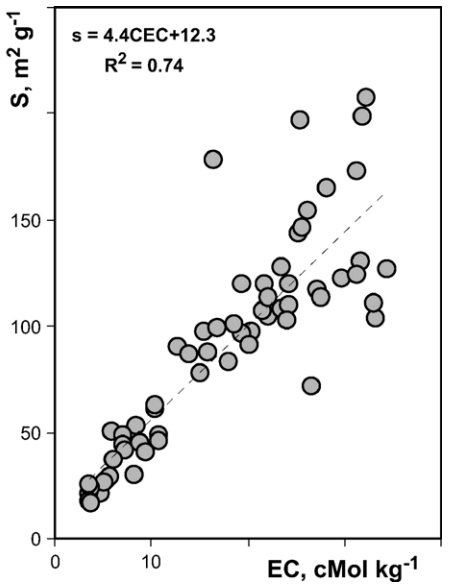

Fig. 8. Dependence of surface area (S) on cation exchange capacity (CEC) for the studied soils.

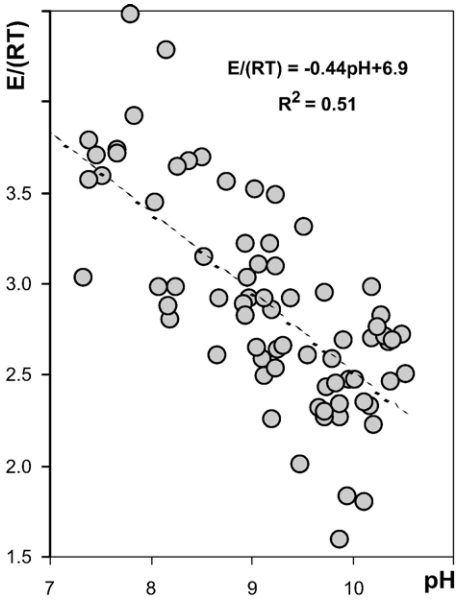

Fig. 10. Dependence of the average adsorption energy (E/RT) on pH for the studied soils.

1981), therefore we looked for dependencies of S and V with parameters of soil salinity. However satisfying correlation occurred only between the sodium saturation percentage (SP) and surface area ($S=1.4SP+8.7$, $R^2=0.53$).

The rise of salinity and sodicity (sodium adsorption ratio) decreases adsorption energy due to lower hydration energy of sodium than the other ions. The only exception is AK soil, having surprisingly the highest values of adsorption energy among strongly salt-affected soils and simultaneously the highest values of sodium adsorption ratio throughout the profile. It is possible that in this highly saline soil the previously mentioned water molecules–salt dissolution process which is as high as this markedly affects the water vapor sorption isotherm even in its beginning. Therefore the adsorption energy of AK includes much larger contribution of the "dissolution energy" than the other soils. Therefore we excluded the AK energy data from the present consideration. This is important to note that among the other parameters calculated from the isotherms, the value of adsorption energy is most sensitive on the presence of salt-dissolution effects. The logarithmic dependence fits best to the experimental data of SAR and E that is illustrated in Fig. 9. As a rule low adsorption energy values ($-E$ below 3) occur for salt-affected soils at the SAR value exceeding around 30. The latter value may possibly be considered as a threshold value of soil salinization. Also, the adsorption energy (all soils) appears to decrease with soil pH (Fig. 10) that seems to be a consequence of the degree of soil salinity, as well.

4. Conclusions

Surface properties of the studied solonetzic soils differ significantly between the soils, in depth of the profile and vary with soil salinity.

Surface properties developed during formation of Solonetz profiles seem to depend on a very complex set of soil physical and chemical variables, which in turn are governed by environmental influences. Among these variables, as this is observed in non-saline soils, cation exchange capacity and granulometric composition play the most important roles. Exchangeable sodium percentage and pH showed significant effect on soil surface energetic character.

Acknowledgements

Authors acknowledge the financial assistance of grants HNSF T25623, T37364 and T37731.

Appendix A

Below we outline briefly the theory and calculation methods used in the present study to estimate soil surface properties from adsorption–desorption data.

A.1. Surface area

The Aranovich (1992) isotherm was used for mathematical description of the adsorption data. A linear form of this equation is:

$$x/\left[a(1-x)^{1/2}\right] = 1/(a_m C) + x/a_m, \quad (1)$$

where $x=p/p_0$ at the temperature of the measurements, a_m [kg kg^{-1}] is the amount of water molecules adsorbed in the first monolayer i.e. the statistical monolayer capacity and $C=\exp(E_a-E_c)/RT$ is the constant related to the adsorption energy, E_a [J mol^{-1}], and the condensation energy of water, E_c [J mol^{-1}] and R is the universal gas constant. Unlike the standard Brunauer–Emmett–Teller (BET) isotherm, the Aranovich isotherm permits the presence of vacancies in the adsorbed layer, is thermodynamically correct and fits the experimental polymolecular adsorption data within a broader range of relative pressures.

After calculation of a_m values from the slopes ($1/a_m$) of Eq. (1), the surface areas of the studied samples, S, were found as:

$$S = L\,\omega\, a_m M^{-1}, \quad (2)$$

where L is Avogadro number, M [kg] is molecular mass of water and ω is the area occupied by a single water molecule equal to $1.08*10^{-19}$ m^2.

Surface areas of the studied soils were calculated from experimental adsorption data for the p/p_0 range between ca. 0.1 to 0.6, basing on Eqs. (1) and (2). In this pressure range the data correlated best ($r^2>0.98$) with the linear form of the Aranovich equation.

A.2. Adsorption energy

Among various models used to find adsorption energy distribution function $f(E)$, (Jaroniec and Brauer, 1986; Polubesova et al., 1997) probably the simplest and reasonably accurate one is to model a complex surface as a combination of energetically homogeneous patches (or randomly distributed sites) having distinct energies. The total water vapor adsorption at a given pressure, $a(p)$, is expressed as a sum of local adsorptions a_i on different sites of energies

$E_i=(E_{a,i}-E_c)$, where $E_{a,i}$ is the adsorption energy of i-th site:

$$a(p)=\sum_{i=1}^{n} a_i(p,E_i), \tag{3}$$

where n is the assumed number of sites. Thus the total adsorption isotherm, $\Theta(p)$, is a sum of adsorptions on all sites, $\Theta_i(p,E_i)$, weighted by their fractions, $f(E_i)$:

$$\Theta(p)=a(p)/a_m=\sum_{i=1}^{n} a_i(p,E_i)/a_{m,i}\left(a_{m,i}/a_m\right)$$

$$=\sum_{i=1}^{n}\Theta_i(p,E_i)f(E_i), \tag{4}$$

where $a_{m,i}$ is the monolayer capacity of sites kind i and values of $f(E_i)$ fulfill normalization condition:

$$\sum_{i=1}^{n} f(E_i)=1. \tag{5}$$

The easiest way to solve Eq. (4) and find site fraction values, $f(E_i)$, goes through a condensation approximation, CA (Harris, 1968). This method is based on the replacement of the true local isotherm by a step-function. Every pressure value becomes associated with the corresponding value of the adsorption energy that provides the adsorption equal to one-half of the adsorption at infinite energy. Following this definition, and using the Aranovich equation for describing local adsorption effects, the final CA formula is:

$$f(E_i)=\left[(1-x_{i+1})^{1/2}\Theta_{i+1}(E_{i+1})-(1-x_i)^{1/2}\Theta_i(E_i)\right]$$
$$/(E_{i+1}-E_i), \tag{6}$$

where $E=-RT\ln(p_0/p)$.

Having calculated $f(E_i)$ values, the average water vapor adsorption energy of the whole adsorbent, E_{av}, can be calculated as:

$$E_{av}=\sum_{i=1}^{n} E_i f(E_i). \tag{7}$$

The calculations of adsorption energy distribution functions were performed using adsorption data and Eq. (6). The energy range (expressed as dimensionless energies in the units of RT, E/RT) varying from 0 to −7 was considered. To convert these dimensionless energies on SI units one shall use the following dependence E_a [kJ mol^{-1}]$=-44+2.48E/RT$, where −44 kJ mol^{-1} is the condensation energy of water vapor and 2.48 kJ mol^{-1}$=RT$ for $T=298$ K. The dimensionless energy equal to 0 holds for energy adsorption equal to the condensation energy of the vapor. $E/RT=-7$ was taken as the maximum adsorption energy. The maximum energy value in the condensation approximation should relate to the minimum value of the p/p_0 applied. The minimum relative pressure in our data sets was around 0.004, which corresponds to the energy adsorption of around −5.5. The condensation approximation allows for the detection of adsorbing sites differing not less than by 1 dimensionless energy unit. Thus it seemed rationale to assume −6 as the maximum energy in the present investigations. However, this value can be considered only as a first estimate of the maximum energy, because of the lack of experimental data at lower then minimum relative pressure. Therefore we arbitrarily took the maximum energy of −7. We thought that if there were no sites with higher adsorption energies than −6 then the corresponding values of $f(E)$ will be close or equal to zero. The value of adsorption at a given energy was found by linear interpolation of the nearest experimental adsorption data. Knowing $f(E_i)$ values, average adsorption energies were calculated from Eq. (8).

A.3. Micropore parameters

From desorption values, characteristics of pores ranging from about 1 to a few tens of nanometers were evaluated (Rouquerol et al., 1995). These pores will be referred to as "micropores". The micropore radius r was related to the vapor pressure p by the Kelvin equation (Oscik, 1979):

$$r=2M\ \sigma\ \cos\alpha/\rho\underline{R}T\ \ln(p_0/p), \tag{8}$$

where M is molecular mass of water, σ is water surface tension, α is a water-solid contact angle (assumed here to be zero), ρ is density of water, $\underline{R}$ is the universal gas constant and T is the temperature of the measurements.

The volume of the condensed water in the pores at a given pressure, $v(p/p_0)$ [m^3], can be treated as a sum of pore volumes, $v_i(r_i)$, of the radii $r_i \le r(p/p_0)$,

$$v(p/p_0)=\sum_{i=1}^{n} v_i(r_i). \tag{9}$$

Dividing the above equation by the total pore volume, v_t, the scaled desorption isotherm, $\Xi(p/p_0)=\Xi(r(p/p_0))$, can be treated as a sum of fractions of particular pores, $f(r_i)$:

$$\Xi(p/p_0)=v(p/p_0)/v_t=\sum_{i=1}^{n} v_i(r_i)/v_t$$

$$=\sum_{i=1}^{n} f(r_i)=1 \tag{10}$$

and the pore fraction in a given range of pore sizes can be calculated as:

$$f(r_{i,\mathrm{av}}) = [\Xi(r_{i+1}) - \Xi(r_i)], \tag{11}$$

where $r_{i,\mathrm{av}}$ denotes the arithmetic mean of r_{i+1} and r_i. Knowing the latter values one easily constructs a pore size distribution function i.e. pore fraction vs. pore radius dependence.

The average pore radii, r_{av}, in the measuring range can be calculated as:

$$r_{\mathrm{av}} = \sum_{i=1}^{n} r_i f(r_i). \tag{12}$$

For the present calculations the condensation in micropores was assumed to occur above $p/p_0=0.35$ (below this value surface adsorption processes dominate) and thus v_t was taken as the volume of adsorbed water at the maximal p/p_0 value applied (0.98) minus that at $p/p_0=0.35$. The latter value was obtained from linear interpolation of the nearest experimental data. For r_{av} determination all experimental data were taken.

The micropore size distribution functions are very sensitive against the experimental errors and precision of the data reading. Therefore we calculated these functions in such way that we broaden the pore ranges for which we calculated $f(r)$ values, until we have similar pore size distribution functions for the replicates of data. This was achieved with four ranges of $\log(r)$. The values of $\Xi(r_{i+1})$ and $\Xi(r_i)$ for the end values of each range were found from linear interpolation of nearest experimental data.

A.4. Surface fractal dimension

Evaluation of the surface fractal dimensions from measured adsorption isotherms was performed employing a well-established method, based on the Frenkel–Hill–Halsey (FHH) adsorption isotherm equation. According to this approach, the experimentally measured adsorption, a, is approximated by using the equation (Neimark, 1990; Jaroniec et al., 1997):

$$\ln(a) = -(1/m)\ln(-\ln(p/p_0)) + C, \tag{13}$$

where C is a constant and the parameter $1/m$ is related to the surface fractal dimension of the sample. Eq. (13) should be applied to the experimental data measured within multilayer adsorption region, i.e. for rather high relative pressures (Neimark, 1990). In this region the effects of energetic surface heterogeneity on adsorption may be neglected, because the surface–adsorbate interactions are screened by the already adsorbed particles.

The determination of the surface fractal dimension, D, requires knowledge of the adsorption regime. The magnitude of the parameter $1/m$ distinguishes two possible adsorption regimes:

1) the van der Waals regime for $1/m<1/3$, yielding the surface fractal dimension $D=3(1-1/m)$;
2) or the capillary condensation regime for $1/m>1/3$, yielding $D=3-1/m$.

Calculations of surface area and fractal dimension requested defining linearity ranges. To do this we used the procedure introduced by Yokoya et al. (1989). According to this procedure the measure of the linearity L for the set of the points in a plane is:

$$L = \left(4\sigma_{xy}^2 + (\sigma_{yy} - \sigma_{xx})^2\right)^{1/2} (\sigma_{yy} + \sigma_{xx})^{-1}, \tag{14}$$

where σ_{xx}, σ_{yy} and σ_{xy} are the variances of x-coordinates, y-coordinates and the covariance between x and y coordinate sets, respectively. The L value falls between 0 (for uncorrelated and random points) and 1 (for points on a straight line). To separate linearity ranges, the value of L is computed for the first three points, then for the first four, five and so on until the value of L increases. The end of the linearity range is in the points after which the value of L begins to decrease. To detect eventually the next linearity range, the procedure is repeated considering the latter points to be the first points of the next linearity interval. Once detected the linearity range, we checked if the linear regression coefficient increases after excluding the first and/or the last point. If so, these points were rejected.

References

Allen, T.F.H., Hoekstra, T.W., 1991. Role of heterogeneity in scaling of ecological systems under analysis. In: Kolasa, J., Pickett, T.A. (Eds.), Ecological Heterogeneity. Springer, N.Y., pp. 47–68.

Anderson, A.N., McBratney, A.B., Crawford, J.W., 1998. Applications of fractals to soil science. In: Sparks, D.L. (Ed.), Advances in Agronomy, vol. 63. Academic Press, pp. 2–76.

Aranovich, G.L., 1992. The theory of polymolecular adsorption. Langmuir 8, 736–739.

Balard, H., Saada, A., Papirer, E., Siffert, B., 1997. Energetic surface heterogeneity of illites and kaolinites. Langmuir 13, 1256–1269.

Chiou, C.T., Lee, J-F., Boyd, A., 1990. The surface area of soil organic matter. Environ. Sci. Technol. 24, 1164–1166.

Coradin, T., Livage, J., 2003. Synthesis and characterization of alginate/silica composites. J. Gel Sci. Technol. 25, 1165–1168.

Gregg, S.J., Sing, K.S.W., 1967. Adsorption, Surface Area and Porosity. Academic Press, London.

Hajnos, M., Sokolowska, Z., Jozefaciuk, G., Hoffmann, C., Renger, M., 1999. Effect of leaching of DOC on pore characteristic of a sandy soil. Z. Pflanzenernähr. Bodenkd. 162, 19–25.

Hajnos, M., Jozefaciuk, G., Sokolowska, Z., Greiffenhagen, A., Wessolek, G., 2003. Water storage, surface, and structural properties of sandy forest humus horizons. J. Plant Nutr. Soil Sci. 166, 625–634.

Harris, L.B., 1968. Adsorption on a patchwise heterogeneous surface. I. Mathematical analysis of the step-function approximation of the local isotherm. Surf. Sci. 10, 129–145.

Hernandez, M.A., 2000. Nitrogen-sorption characterization of the microporous structure of clinoptiolite-type zeolites. J. Porous Mater. 7, 443–454.

Hoffmann, C., Renger, M., Hajnos, M., Sokolowska, Z., Jozefaciuk, G., Marschner, B., 1999. Reactions of sewage farm soils to different irrigation solutions in a column experiment: 1. Solid phase physicochemical properties. Z. Pflanzenernähr. Bodenkd. 162, 653–659.

Jaroniec, M., Brauer, P., 1986. Recent progress in determination of energetic heterogeneity of solids from adsorption data. Surf. Sci. Rep. 6, 65–117.

Jaroniec, M., Kruk, M., Olivier, J., 1997. Fractal analysis of composite adsorption isotherms obtained by using density functional theory data for argon in slitlike pores. Langmuir 13, 1031–1035.

Jozefaciuk, G., Bowanko, G., 2002. Effect of acid and alkali treatment on surface areas and adsorption energies of selected minerals. Clays Clay Miner. 50, 771–783.

Jozefaciuk, G., Sokolowska, Z., 2003. The effect of removal of organic matter, iron oxides and aluminum oxides on the micropore characteristics of the soil clay fraction. Pol. J. Soil Sci. XXXVI/2, 111–120.

Jozefaciuk, G., Sokolowska, Z., Sokolowski, S., Alekseev, A.O., Alekseeva, T.P., 1995. Changes of mineralogical and surface properties of water dispersible clay after acid treatment of soils. Clay Miner. 30, 149–155.

Jozefaciuk, G., Sokolowska, Z., Hajnos, M., Hoffmann, C., Renger, M., 1996. Effect of leaching of DOC on water adsorption properties of sandy soil. Geoderma 74, 125–137.

Jozefaciuk, G., Hoffmann, C., Renger, M., Marschner, B., 2000. Effect of extreme acid and alkali treatment on surface properties of soils. J. Plant Nutr. Soil Sci. 163, 595–601.

Jozefaciuk, G., Muranyi, A., Szatanik-Kloc, A., Farkas, C., Gyuricza, C., 2001. Changes of surface, fine pore and variable charge properties of a brown forest soil under various tillage practices. Soil Tillage Res. 59, 127–135.

Jozefaciuk, G., Hoffmann, C., Marschner, B., 2002. Effect of extreme acid and alkali treatment on pore properties of soil samples. J. Plant Nutr. Soil Sci. 165, 59–66.

Jozefaciuk, G., Muranyi, A., Fenyvesi, E., 2003. Effect of randomly methylated beta-cyclodextrin on physical properties of soils. Environ. Sci. Technol. 37, 3012–3017.

Lipiec, J., Hatano, R., Slowinska-Jurkiewicz, A., 1998. The fractal dimension of pore distribution patterns in variously-compacted soil. Soil Tillage Res. 47, 61–66.

Neimark, A.V., 1990. Determination of surface fractal dimension from the results of an adsorption experiment. Russ. J. Phys. Chem. 64, 1398–1403.

Newman, A.C.D., 1983. The specific surface of soils determined by water sorption. J. Soil Sci. 34, 23–32.

Oscik, J., 1979. Adsorpcja. PWN, Warszawa (in Polish).

Pachepsky, Y.A., Polubesova, T.A., Hajnos, M., Jozefaciuk, G., Sokolowska, Z., 1995a. Parameters of surface heterogeneity from laboratory experiments on soil degradation. Soil Sci. Soc. Am. J. 59, 410–417.

Pachepsky, Y.A., Polubesova, T.A., Hajnos, M., Sokołowska, Z., Józefaciuk, G., 1995b. Fractal parameters of soil pore area as influenced by simulated soil degradation. Soil Sci. Soc. Am. J. 59/1, 68–75.

Pennell, K.D., Boyd, S.A., Abriola, L.M., 1995. Surface area of soil organic matter reexamined. Soil Sci. Soc. Am. J. 59, 1012–1018.

Perfect, E., Kay, B.D., 1995. Application of fractals in soil and tillage research: a review. Soil Tillage Res. 36, 1–20.

Petersen, L.W., Moldrup, P., Jacobsen, O.H., Rolston, D.E., 1996. Relation between soil specific area and soil physical and chemical properties. Soil Sci. 161, 9–21.

Polubesova, T.A., Pachepsky, Y.A., Hajnos, M., Jozefaciuk, G., Sokolowska, Z., 1997. Comparison of three techniques to assess surface heterogeneity of solids in soils. Int. Agrophys. 11, 189–198.

Rouquerol, J., Avnir, D., Fairbridge, C.W., Everett, D.H., Haynes, J.H., Pernicone, N., Ramsay, J.D.F., Sing, K.S.W., Unger, K.K., 1995. Recommendations for the characterization of porous solids. (Technical Report). Pure Appl. Chem. 66, 1739–1758.

Senesi, N., 2000. Fractal in general soil science and in soil biology and biochemistry. Soil Biol. 9, 415–472.

Sequi, P., Aringhieri, R., 1977. Destruction of organic matter by hydrogen peroxide in the presence of pyrophosphate and its effect on the soil specific surface. Soil Sci. Soc. Am. J. 41, 430–432.

Sokolowska, Z., 1989. On the role of energetic and geometric heterogeneity in sorption of water vapour by soils. Geoderma 45, 251–265.

Sokolowska, Z., Sokolowski, S., 1999. Influence of humic acid on surface fractal dimension of kaolin: analysis of mercury porosimetry and water adsorption data. Geoderma 88, 233–249.

Sokolowska, Z., Jozefaciuk, G., Sokolowski, S., Renger, M., Wilczynski, A., 1993a. Water vapour adsorption as related to liming of acidic sandy forest soils. Z. Pflanzenernähr. Bodenkd. 156, 495–499.

Sokolowska, Z., Jozefaciuk, G., Sokolowski, S., Urumova-Pesheva, A., 1993b. Adsorption of water vapour on soils: the influence of organic matter and the components of iron and aluminum on energetic heterogeneity of soil samples. Clays Clay Miner. 41, 346–352.

Sokolowska, Z., Hajnos, M., Jozefaciuk, G., Hoffmann, C., Renger, M., 1997. Influence of humic acid on water adsorption characteristics of kaolin and quartz. Z. Pflanzenernähr. Bodenkd. 160, 327–331.

Sokolowska, Z., Hajnos, M., Dabek-Szreniawska, M., 1999. Relation between adsorption of water vapour, specific surface area and soil cultivation. Pol. J. Soil Sci. XXXII/2, 3–12.

Sokolowska, Z., Hajnos, M., Bowanko, G., 2000. Nitrogen adsorption study of the surface properties of the secondary transformed peat-moorsh soils. Acta Agrophys. 26, 65–73.

Tombacz, E., Szekeres, M., Baranyi, L., Micheli, B., 1998. Surface modification of clay minerals by organic polyions. Colloids Surf. 141, 379–384.

Toth, T., Jozefaciuk, G., 2002. Physicochemical properties of a solonetzic toposequence. Geoderma 106 (1–2), 137–159.

Toth, T., Kuti, L., Kabos, S., Pasztor, L., 2001. Use of digitalized hydrogeological maps for evaluation of salt-affected soils of large areas. Arid Land Res. Manag. 15, 329–346.

Varallyay, G., 1981. Extreme moisture regime as the main limiting factor of soil fertility of salt affected soils. Agrokém. Talajt. 30, 73–96.

Walczak, R.T., Witkowska-Walczak, B., Slawinski, C., 2002. Comparison of correlation models for the estimation of the water retention characteristics of soils. Int. Agrophys. 16, 79–82.

Wilczynski, W., Renger, M., Jozefaciuk, G., Hajnos, M., Sokolowska, Z., 1993. Surface area and CEC as related to qualitative and quantitative changes of forest soil organic matter after liming. Z. Pflanzenernähr. Bodenkd. 156, 235–238.

Yokoya, N., Yamamato, K., Funakuro, N., 1989. Fractal-based analysis and interpolation of 3D natural surface shapes and their application to terrain modelling. Comput. Vis. Graph. Image Process. 46, 284–302.